J Mater Sci (2010) 45:3497–3505
DOI 10.1007/s10853-010-4386-7

Surface-sulfonated polystyrene microspheres improve crack resistance of carbon microfiber-reinforced Portland cement mortar

Zhengxian Yang · John Hollar · Xianming Shi

Received: 2 December 2009 / Accepted: 4 March 2010 / Published online: 19 March 2010

Abstract The formation of microcracks is a major concern for the integrity and durability of concrete and other cementitious composites, since such microcracks cannot be easily controlled and detected within the matrix of composite. This work explored the possibility of using surface-sulfonated polystyrene microspheres (SPSM) featuring an average diameter of 0.7 ± 0.5 μm to improve the crack resistance of carbon microfiber-reinforced mortar. The compressive strength and EIS data demonstrated that the incorporation of SPSM at 0.15% by weight of cement led to a denser and more refined microstructure of the cement mortar composite, likely attributable to the active interactions between SPSM and cement hydration products as well as carbon microfibers. The crack resistance of these cement-based composites was evaluated using a non-destructive test under uniaxial compression loading along with a fatigue test under uniaxial compression cyclic loading. The data, in the form of critical stress, specific crack area, and fatigue strain, revealed that even at a small dosage the incorporation of SPSM to carbon microfiber-reinforced mortar retarded the initiation of unrecoverable microcracks and slowed down the propagation of microcracks under uniaxial compression loading, and improved the crack resistance and toughness of the specimens under fatigue loading.

Z. Yang · J. Hollar · X. Shi (✉)
Corrosion and Sustainable Infrastructure Laboratory, Western Transportation Institute, College of Engineering, Montana State University, P.O. Box 174250, Bozeman, MT 59717-4250, USA
e-mail: xianming_s@coe.montana.edu

X. Shi
Civil Engineering Department, Montana State University, 205 Cobleigh Hall, Bozeman, MT 59717-2220, USA

Introduction

Cracking is a major culprit for the premature deterioration of structures and buildings made of concrete or other cement-based materials. Both conventional concrete and high performance concrete are inherently brittle and tend to crack under stress, posing a risk for the durability, reliability, serviceability, and even safety of concrete infrastructure [1]. The direct and indirect costs of concrete cracking are substantial, as it entails additional repair, rehabilitation, and monitoring activities to ensure the functionality and aesthetics of concrete structures and components. A recent estimate from the industry places early age cracking as a $500 million problem in the U.S. alone, not to mention other types of cracking that can occur at different stages in the service life of concrete infrastructure [2].

Microcracks often develop in cementitious composites as a result of mechanical loadings (static or cyclic), environmental loadings (e.g., freezing and thawing, rebar corrosion, alkali aggregate reactions, sulfate attack), and volumetric instability (e.g., shrinkage in fresh or hardened concrete, thermal contraction). Once formed, they are extremely difficult to be detected and repaired by conventional methods before they develop, coalesce and grow into macrocracks. For prestressed or reinforced concrete structures, cracking of the concrete accelerates the ingress of water, chlorides, and other deleterious species and further undermines the integrity of the structure through aggravated corrosion of the metal inside concrete. As such, both microcracks and macrocracks can compromise the ability of the structure to withstand loads, which eventually leads to structural failure.

In recent years, the use of various natural or synthetic short fibers to reinforce cementitious composites and other

types of composite materials has gained popularity, as fibers feature the strain-hardening behavior associated with the enhancement of tensile/flexural strength and fracture toughness [3–9]. On the other hand, the incorporation of electrically conductive short fibers (e.g., carbon microfibers) to cementitious materials can endow them with enhanced electrical conductivity and lower activation energy in certain temperature ranges, which subsequently opens up a wide array of non-structural applications [10, 11]. Owing to their small diameter and high aspect ratio, short fibers have a large numerical density in the matrix even when admixed at relatively low volume fractions and thus have the potential to interact with microcracks formed in composite materials. As such, short fibers have been proven to effectively flank and bridge microcracks before they become coalescent and form macrocracks [9, 12]. The admixing of short fibers in cementitious composites has shown many prospective benefits, but the effectiveness hinges on the uniform dispersion of fibers in the matrix.

The use of polymer as a modifier in new structures has also been proven to be a promising strategy in improving the microstructure and durability of cement mortar and concrete [13–15]. As a thermoplastic polymeric material, plastic granules of polystyrene have been used as lightweight aggregate to produce low-density concrete and as a good thermal insulation material required for some specialized building applications [16–18]. In fields other than civil engineering, monodispersed microspheres of polystyrene have also been widely used for a long time [19, 20]. Nonetheless, little research has been conducted to examine the use of polystyrene microspheres in cement-based materials or to investigate the possible synergy between such microspheres and short fibers in improving the crack resistance of cement-based materials.

This work aimed to evaluate the feasibility of using surface-sulfonated polystyrene microspheres (SPSM) featuring an average diameter of 0.7 ± 0.5 μm to improve the crack resistance of carbon microfiber-reinforced cementitious composites. Various experiments, including compressive strength test, microcracking evaluation under uniaxial compressive loading, fatigue test under uniaxial cyclic loading, and electrochemical impedance spectroscopy (EIS) measurements were carried out to investigate the properties of these cementitious composites with or without the SPSM admixed.

Experimental

Materials

Commercially available styrene monomers and concentrated sulfuric acid (98%) were obtained from Fisher Scientific Inc. and used without further purification. Analytical grade dimethyl sulfoxide (DMSO), methanol, ethanol, and sodium hydroxide were also obtained from Fisher Scientific Inc. and used as received. Deionized water (resistivity > 18.2 MΩ cm^{-1}) prepared by Milli-Q 185 system (Millipore, USA) was used for all experiments. The carbon microfibers were KRECA chop C-103T, 3 mm in length with a filament diameter of 18 μm, as obtained from Kureha Co. (Tokyo, Japan). ASTM C1240 silica fume obtained from BASF/MB admixtures, Inc. (Henderson, NV) was used as a dispersant for the fibers in the mixes. The basic physical properties of the fibers are shown in Table 1. ASTM C150-07 Type I/II low-alkali Portland cement (ASH Grove Cement Company, Clancy, MT, USA) was used in our study. The chemical composition and physical properties of the cement were presented in a previous reference [15]. The fine aggregate used was river sand sifted to allow a maximum aggregate size of 1.18 mm. Before proportioning and admixing, the aggregate was pretreated and taken to a saturated surface dry (SSD) condition.

Table 1 Basic physical properties of carbon microfibers

Property	Test result
Tensile strength	670 MPa
Tensile elastic modulus	30 GPa
Elongation	2.2%
Volume resistivity	150 μΩ
Specific gravity	1.63
Thermal conductivity	5–10 W/m/K
Carbon content	Min 95 wt%
Oxidation onset temperature	310 °C

Preparation of surface-sulphonated polystyrene microspheres

Monodispersed polystyrene microsphere powder was prepared by radiation-induced dispersion polymerization as described elsewhere [21]. The polystyrene microspheres were sulphonated in concentrated sulfuric acid for 60 h at 40 °C. After diluting, the sample was repeatedly centrifuged, washed with ethanol–water, and then dried in vacuum.

Preparation of mortar specimens

All specimens were prepared in a rotary mixer with a flat beater at a constant water-to-binder mass ratio of 0.52 and a constant sand-to-binder mass ratio of 2. The carbon microfiber content in the mortar mix was 2.0% by volume. The silica fume as a dispersant was used in the amount of 15% by weight of cement. SPSM powder was used in the

amount of 0.15% by weight of cement and first dissolved in water and then sodium hydroxide was added. The mixture was then stirred to obtain a homogeneous solution with a final pH value around 8. Then this mixture (if applicable) was used with mixing water in the preparation of mortar specimens. For both the control (without SPSM admixed) and SPSM mortar specimens (with SPSM admixed), three or more specimens were fabricated for each test to ensure the statistical reliability of the test results. The mixing sequence was the following: the cement, silica fume, and mixing water were first mixed to form a paste, and then the fibers were slowly added while mixing continued, and finally the sand was incorporated. After mixing, the fresh mixture was cast into molds to form Φ50 × 100 mm cylinders, and was carefully compacted to minimize the amount of entrapped air. The mortar specimens were de-molded after 24 h and then cured in a wet chamber (20 ± 2 °C, relative humidity > 95%) for 27 additional days, before being subjected to the tests.

Characterization and property testing

FESEM imaging of SPSM

At the completion of the SPSM fabrication, a Zeiss Supra 55VP PGT/HKL FESEM system was employed to examine the morphology of the SPSM.

Compressive strength testing of mortar specimens

The compressive strength test was carried out by breaking cylindrical mortar specimens in a hydraulic Material Testing System (MTS Model 880) using a loading rate of 64 lbf/s, and the load and displacement data were automatically recorded. The ultimate compressive strength was then calculated by dividing the load at failure by the cross-sectional area resisting the load. In our study, the specimens cured for 1 day and 28 days after casting were surface-ground to ensure their square dimensions and then polished with fine silicon carbide paper before being subjected to the compressive strength test to ensure a uniform surface finish (and thus a uniformly distributed load). The test results are the average of at least three specimens made from the same batch mixture and tested at the same age.

Microcrack evaluation during the uniaxial compression loading

Many different methods have been developed to investigate the microcracking or cracking in cement-based materials over the last several decades. In our study, we used the non-destructive method of microcrack evaluation proposed by Loo [22] to evaluate the microcracking in mortar specimens during the uniaxial compression test. The method provides a quantitative indication of the extent of microcracking in a prismatic concrete specimen under uniaxial compression. The formula was derived on the assumption that the change in cross-sectional area of a prismatic concrete specimen during the test equals the sum total of the elastic change in cross-sectional area due to Poisson's ratio effects and the dilation due to microcracking. Thus,

$$\Delta A_{\mathrm{T}} = \Delta A_{\mathrm{PR}} + \Delta A_{\mathrm{C}},$$

where ΔA_{T} is the total change in cross-sectional area of concrete, ΔA_{C} the change in cross-sectional area due to microcracking, and ΔA_{PR} is the change in cross-sectional area due to Poisson's ratio effects. For the case of concrete cylinders

$$A = \pi r^2,$$

where A is the cross-sectional area of cylinder and r is radius of cylinder. Based on this assumption, the specific crack area ($\varepsilon_{\mathrm{cr}}$) of cylindrical specimens can be estimated by the equation below:

$$\varepsilon_{\mathrm{cr}} = 2\left(\varepsilon_x - \mu\varepsilon_y\right), \quad \mu = g_y/g_x,$$

where ε_x and ε_y are the transverse and axial strains, respectively, μ is the elastic Poisson's ratio, g_x and g_y are the gradients of the linear portion in the stress–transverse–strain curve and stress–axial–strain curve, respectively. The specific crack area has the same unit as the ε_x and ε_y, and is expressed in microstrain.

After curing for 28 days, one CEA-06-250UT-350 90° foil strain gage rosette from Vishay Micro-Measurements group, Inc. (Raleigh, NC) was attached to each specimen at mid-height, allowing for the measurement of strain in both the axial and transverse direction. Both the axial and transverse gages had a gage length of 6.35 mm, and a gage factor of 2.090 ± 0.5% and 2.110 ± 0.5%, respectively. The specimens were then placed between two steel platens mounted in a hydraulic Material Testing System (MTS Model 880) and progressively loaded from 30 to 90% of their static ultimate compressive strength (f_{c}') in increments of 5%. Strain data was recorded using a Campbell Scientific® CR5000 data logger. A ram displacement of 0.09 mm/min for loading and 2.0 mm/min for unloading was used. The specimen was unloaded immediately after reaching the determined load, and the next loading cycle was delayed until the change in strain recovery was negligible.

Fatigue test under uniaxial compression cyclic loading

The cylindrical mortar specimens were first loaded to 80% of their static ultimate compressive strength using a

hydraulic Material Testing System (MTS Model 880) and then cyclically loaded between 25 and 95% of their static ultimate compressive strength until failure. Fatigue strain data was recorded using a strain gage from Vishay Micro-Measurements group, Inc. (Raleigh, NC). As the maximum aggregate size used was 1.18 mm in diameter, a gage length of 6.35 mm (larger than the minimum recommendation of 5.89 mm) was deemed sufficient. The frequency of loading was 1 Hz, and was applied sinusoidally with time. Data was recorded using a Campbell Scientific® CR5000 data logger. A Tektronix® CPS250 power supplier was used to supply power to the strain gage circuitry. The voltage supplied by the CPS250 was 12 V but was regulated down to 5 V and was applied across a 350Ω-resistor Wheatstone bridge.

Electrochemical impedance measurements

A Gamry Reference 600™ Potentiostat/Galvanostat/ZRA instrument was employed to measure electrochemical impedance spectra of mortar specimens in order to characterize their microstructural properties. To evaluate the microcracking effect in mortar specimens, electrochemical impedance measurements were conducted at 28 days and just after the samples were loaded to 80% of their ultimate compressive strength using specimens prepared from the same batch of mixture. All the EIS measurements were carried out in a local-room air environment (relative humidity around 15–20%, temperature 20 ± 2 °C). The experimental setup is illustrated in Fig. 1.

The ends of the specimen were carefully polished and coated with a layer of silver paint and then a carbon conductive sheet was adhered to eliminate possible errors resulting from poor contact between the specimen and electrodes. The EIS measurements were taken by polarizing the working electrode at ±10 mV around its open circuit potential (OCP), using sinusoidal perturbations with a frequency between 1 MHz and 0.01 Hz (10 points per decade). The Gamry Echem Analyst™ software was used to plot and fit the data.

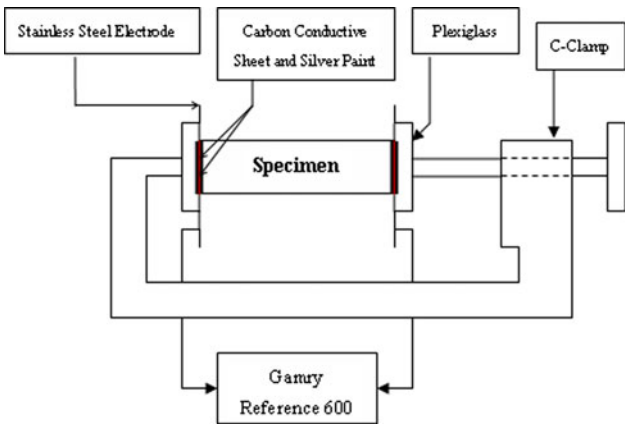

Fig. 1 Schematic illustration of experimental setup for electrochemical impedance measurements of mortar specimen

Results and discussion

Morphology of the SPSM

The morphology of SPSM was examined by FESEM as shown in Fig. 2. We used Adobe Photoshop CS4 software to measure at least 100 microspheres in the photos and discovered that the diameter of the SPSM had an average value of 0.7 ± 0.5 μm.

Compressive strength of the mortar

Compressive strength test results of the two types of mortar specimens at 1-day and 28-day curing ages are illustrated in Fig. 3. Relative to the control, the SPSM specimens showed a higher compressive strength at both 1 day and 28 days for the given mixing proportion (i.e. water-to-binder ratio of 0.52, sand-to-binder ratio of 2, silica fume at 15% by weight of cement, and carbon microfibers at 2% by volume). In particular, the incorporation of SPSM at 0.15% by weight of cement increased the 1-day and 28-day compressive strength of the mortar by 22.2 and 14.8% respectively.

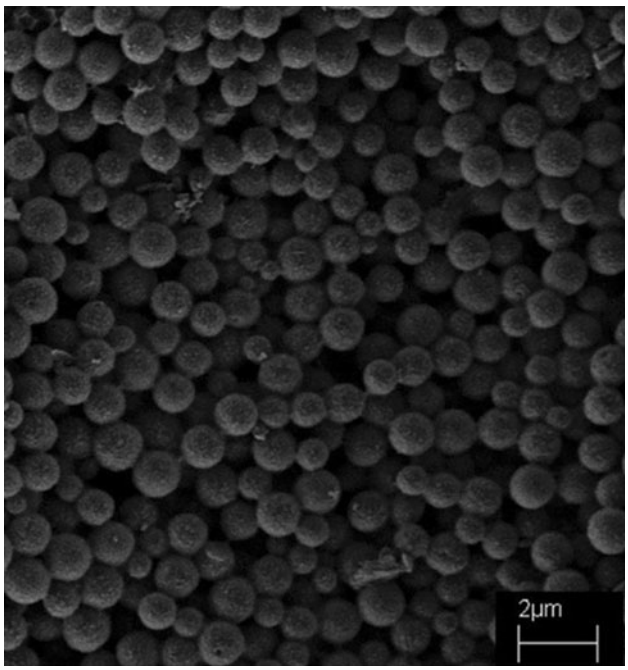

Fig. 2 Typical FESEM photograph of surface-sulfonated polystyrene microspheres

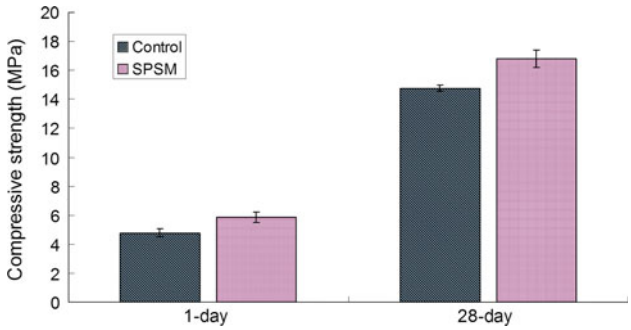

Fig. 3 Compressive strength of mortar specimens with SPSM and without SPSM admixed (control) at 1-day and 28-day curing ages

Microcracking behavior of the mortar

Critical stress

The critical stress (σ_{cs}) corresponds to the maximum value of volumetric strain at which the stress–volumetric strain curve deviates from linearity and the volume of the specimen starts to expand rather than continuing to decrease. A study of the correlation between external volume changes and internal microcrack propagation in mortar and concrete specimens showed that the critical stress indicates the onset of unstable or unrecoverable microcrack propagation and is related to a significant increase of microcracks throughout the matrix [23, 24]. The variation of axial, transverse, and volumetric strain during the uniaxial compression loading through the non-destructive method of microcrack evaluation was analyzed and is presented in Fig. 4. Volumetric strain was calculated from the small strain relation: $\Delta V/V = \varepsilon_x - 2\varepsilon_y$ and the critical stress is indicated by a horizontal arrow on the volumetric strain curve. As shown in Fig. 4, relative to the control, the incorporation of SPSM (0.15% by weight of cement) increased the critical stress of mortar specimens from 0.78 to 0.86. This 10.3% increase shows a notable effect of SPSM on retarding the initiation of unrecoverable microcracks in the cementitious composite matrix and thus improving its crack resistance.

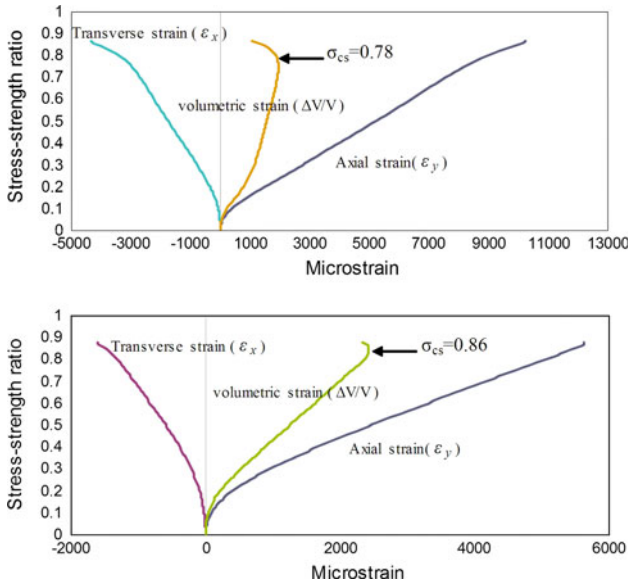

Fig. 4 The variation of axial, transverse, and volumetric strain during uniaxial compression loading of control (*top*) and SPSM (*bottom*) mortar specimens

Specific crack area

Results of specific crack areas were calculated from the strain data using the non-destructive method of microcrack evaluation and plotted against the corresponding stress–strength ratios as shown in Fig. 5. The initiation stress is the point beyond which microcracks begin to propagate in mortar or concrete. This can be determined from the curves in Fig. 5 as the point when the curve begins to deviate from the initial vertical line. In our study, the initial stress of the control and SPSM mortar specimens was found to be 15 and 25% of their respective static ultimate compressive strengths, suggesting the beneficial role of SPSM in slowing down the propagation of microcracks in the cementitious composite under uniaxial compression loading. Another observation is related to the acceleration of microcracking with stress beyond the initial stress. As can be seen in Fig. 5, the curve of stress versus specific crack area of the control samples bends much more sharply toward the crack axis, corresponding to a significant increase in the level of cracking. Relative to the control, the specific crack area of the mortar specimen with SPSM admixed at 0.15% by weight of cement increased slowly as the stress–strength ratio increased from 30 to 90%, indicating a significant decrease in crack initiation and propagation in the SPSM specimen under progressively increasing loads.

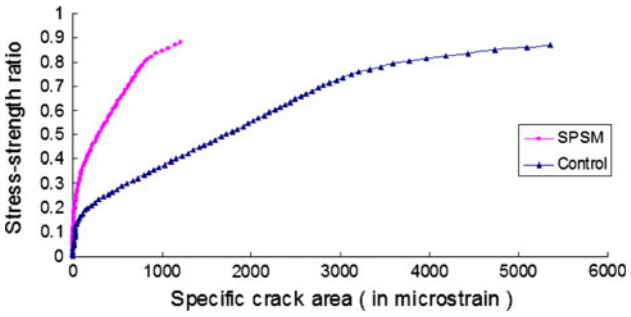

Fig. 5 Relationship between specific crack area and stress–strength ratio for control and SPSM mortar specimens under uniaxial compression loading

Fatigue behavior of the mortar

Fatigue is progressive and permanent internal damage in a material subjected to repeated loading. This is attributed to the propagation of internal microcracks which results in a significant increase of irrecoverable strain. In general, fiber-reinforced concrete is used as paving material for airfields, highways, bridge decks, and industrial floors, which experience significant cyclic loadings during their service lives. The use of fibers in engineering applications has promoted the need to study their fatigue behavior under cyclic loading. Previous studies have found that the addition of fibers can benefit the fatigue performance of concrete [25]. However, the benefit under compressive fatigue loading derived from the addition of fibers is not as significant as that under the flexural fatigue loading. In addition, it has been suggested that the presence of fibers only help to enhance the fatigue behavior in low cycle regions and is limited in providing any improvement at a higher number of cycles [26, 27]. In our study, the typical history of fatigue behavior of both control and SPSM specimens under uniaxial compression cyclic loading was depicted by the relationship between the number of loading cycles until failure and the fatigue strain as shown in Fig. 6. It was found that the fatigue strain development of both types of specimens featured three definite stages: the first stage is the quick strain increase up to about 10% of the total life, the second stage attributed to the development of a large amount of small cracks in matrix features the gradual strain increase from 10% to about 80% of total life, and the last stage is another quick strain increase until failure. Relative to the control, the SPSM specimen has a significantly prolonged second stage of its curve, illustrating the beneficial role of SPSM in inhibiting the initiation and propagation of cracks. This also translates to higher load carrying capacity of fiber-reinforced mortar specimens when they are admixed with SPSM even at a relatively small dosage. Relative to the control, the SPSM specimen has smaller fatigue strain after the same number of load cycles and its strain increment curve is less steep, illustrating the beneficial role of SPSM in enhancing the toughness of the cementitious composite under fatigue loading.

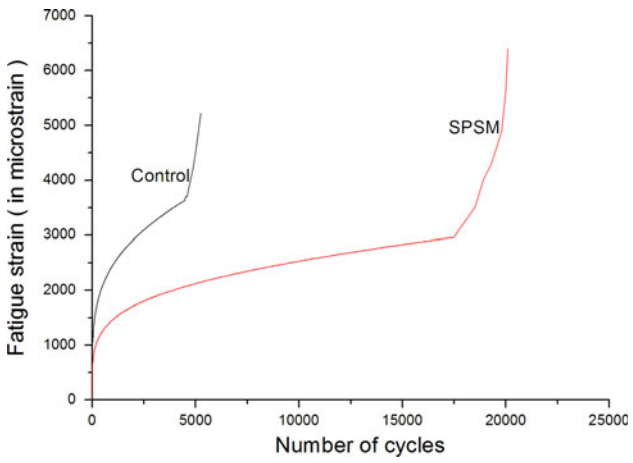

Fig. 6 Relationship between fatigue strain and the number of cycles for control and SPSM mortar specimens under uniaxial compression cyclic loading

Electrochemical characterization of the mortar

As a non-destructive test method, EIS has been found to be effective in revealing the microstructure of cementitious composites [28–31] and thus was utilized to shed light on the microstructural properties of the fiber-reinforced cement mortars in our study. The complex impedance of the composite material depends on the frequency of an externally imposed alternating current (AC) polarization signal, allowing for the representation of a system with an equivalent circuit typically consisting of resistors and capacitors. The equivalent circuit (upper) and the microstructure of a mortar specimen (lower) shown in Fig. 7 were used to interpret the EIS data. Constant phase elements (Q) instead of pure capacitors were used in this equivalent circuit. Such modification is obligatory when the phase angle of capacitor is different from $-90°$.

As shown in Fig. 7 (lower), there are three kinds of paths in such a carbon microfiber-reinforced mortar structure: continuous conductive paths (CCPs), discontinuous conductive paths (DCPs), and matrix conductive paths. The CCPs are the continuously connected pores or microcracks in the mortar microstructure, whereas the DCPs are the discontinuous pores or cracks whose continuity is blocked by the cement paste layers denoted as "discontinuous points" (DPs). Apart from the DCPs and CCPs, the mortar matrix consisting of cement paste particles and carbon microfibers, can act as another kind of conductive path. Based on the above considerations, the EIS parameters we used to represent the microstructure of fiber-reinforced mortar were: R_{mat}, R_{CCP}, and R_{CP}, the resistances of the mortar matrix and that of the continuously and discontinuously connected pores or cracks in the mortar, respectively; Q_{mat} and Q_{dp}, the constant phase element (in place of pure capacitance) across the mortar matrix and that of the cement paste layers blocking the discontinuously connected pores or cracks (i.e., "discontinuous points") in the mortar, respectively. In addition, we assigned the Warburg impedance (W) to one electrode/mortar interface characterizing the diffusion of species through the interface and R_0 to represent the total resistance of metal electrodes, carbon conductive sheet, and electrical wires in the designated circuit.

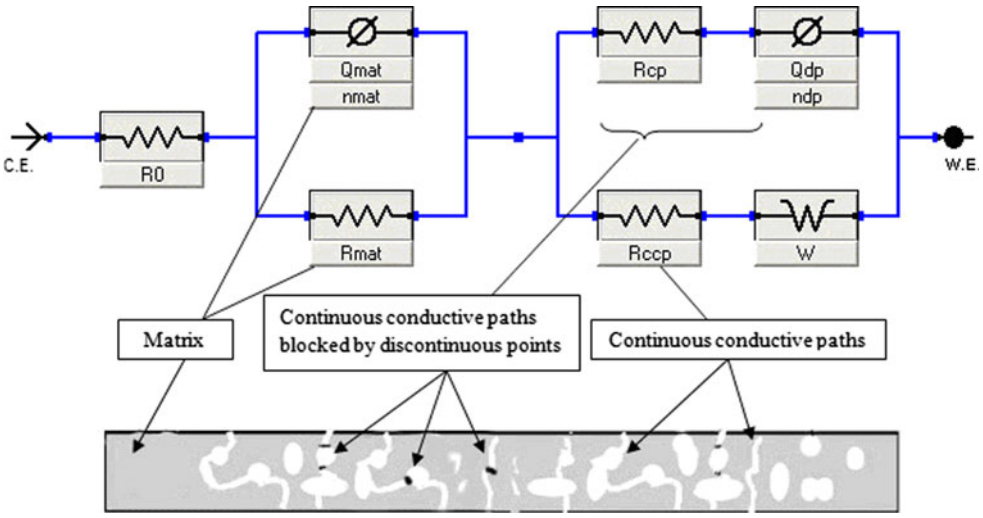

Fig. 7 The equivalent circuit and the microstructure of mortar specimen used for fitting the impedance spectra

Table 2 Equivalent circuit parameters of the carbon microfiber-reinforced mortar specimens at various experimental stages

Testing time	28-day curing age		28-day curing age after 0.8 f_c'	
Specimen	Control	SPSM	Control	SPSM
R_{mat} (Ω cm^2)	583 ± 12.2	585 ± 8.24	483 ± 8.91	473 ± 1.66
Q_{mat} (nScm^{-2})	19.3 ± 4.99	5.28 ± 0.31	20.2 ± 2.91	6.91 ± 1.77
n_{mat}	0.81 ± 0.09	0.99 ± 0.01	0.68 ± 0.03	0.97 ± 0.03
R_{CCP} (kΩ cm^2)	11.1 ± 0.41	13.4 ± 0.25	2.73 ± 0.13	6.28 ± 0.32
R_{CP} (Ω cm^2)	209 ± 3.00	333 ± 11.2	33.2 ± 1.38	99.3 ± 3.54
Q_{dp} (μScm^{-2})	6.04 ± 0.73	4.65 ± 0.02	12.7 ± 1.25	8.27 ± 0.04
n_{dp}	0.52 ± 0.00	0.51 ± 0.00	0.52 ± 0.00	0.47 ± 0.00

The electrochemical impedance measurements began just after the samples were cured for 28 days. Table 2 shows the key equivalent circuit parameters of the two kinds of mortar specimens at two experimental stages designed to investigate the cracking behavior in mortar specimens, in which n ($0 < n < 1$) is the fitting coefficient for Q, the constant phase element (with 1 being the perfect fit of a capacitor and 0 being the worst). All of the "Goodness of Fit" was found to be in the acceptable range. R_0 ranged from 0.62 to 3.22 Ω cm^2 and W ranged from 157 to 785 μScm^{-2}.

The parameters R_{CCP}, R_{CP}, Q_{dp}, and n_{mat} are characteristic of the microstructure of the cementitious composite defined by the pores, cracks, and possibly air voids. As shown in Table 2, relative to the control, the 28-day SPSM specimen had higher values of R_{CCP} and R_{CP} as well as lower values of Q_{dp}. This observation, along with the increased n_{mat} and decreased capacitance Q_{mat} of the SPSM specimens, suggests that the incorporation of SPSM led to a denser and more refined microstructure of the cementitious composite. This is consistent with the findings related to increased compressive strength and reduced specific crack area during compression loading of the SPSM mortar specimens, discussed in previous sections (also shown in Figs. 3, 5).

At the completion of the first EIS measurements at the 28-day curing age, both control and SPSM specimens were loaded under 80% of their ultimate compressive strength to generate artificial microcracks in them and subsequently, the EIS measurements were performed. As shown in Table 2, compared with the mortar specimens prior to this significant loading, the mortar specimens after the loading showed lower n_{mat}, R_{CCP}, and R_{CP} values and higher Q_{mat} and Q_{dp} values, indicative of the compromised integrity of their microstructure resulting from artificial cracks. During the process of compressive loading, some continuously connected micro-pores or microcracks may transform into the discontinuously connected micro-pores or microcracks blocked by cement paste layers, whereas some blocked discontinuously connected micro-pores or microcracks may become continuously connected in such a short fiber-reinforced mortar system. Therefore, in this case, the total

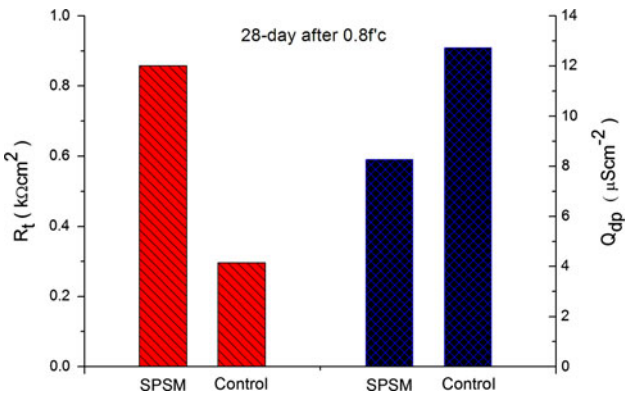

Fig. 8 Resistance (R_t, *left*) and capacitance (Q_{dp}, *right*) values at the 28-day curing age after the mortar specimens being loaded to 80% of ultimate compressive strength

resistance values of R_{CCP} and R_{CP} instead of individual resistance values would be a better indicator of the changes in the composite microstructure.

The total resistance value (R_t) calculated as $R_{CCP}R_{CP}/(R_{CCP} + R_{CP})$ and the capacitance of discontinuous points (Q_{dp}) at the 28-day curing age after being loaded to 80% of compressive strength are depicted in Fig. 8. After this significant loading, the SPSM specimen exhibited higher R_t value and lower Q_{dp} value relative to the control. Since R_t represents the total resistance of the micro-pores and microcracks and Q_{dp} represents the capacitance of the cement paste layers blocking the discontinuously connected micro-pores or microcracks, this observation confirms the beneficial role of SPSM in reducing the level of cracking in the cementitious composite under compressive loading. These data suggest that after the loading the SPSM-modified composite had lower number of cracks and/or smaller cracks formed in the matrix relative to the control.

Possible role of the SPSM in cementitious composite

There are multiple mechanisms that may account for the beneficial effects of the incorporation of SPSM in the cementitious composite investigated in this specific study. First, these microspheres (SPSM) can serve as micro-fillers and fill in the voids within the hydrated cement paste and at the interface of cement paste and microfibers, leading to denser microstructure of the cementitious composite. Second, these microspheres can participate in the cement hydration process at the microscopic level as shown in Fig. 9. The substitution of Na^+ by Ca^{2+} and the binding of Ca^{2+} to two adjacent monobasic groups would act to promote the precipitation of calcium-rich hydration products which provide the chemical interlocking responsible for the development of cement–fiber interfacial bonds and therefore improving the mechanical properties of fiber-reinforced cement mortar. Third, these microspheres along with the silica fume particles are expected to assemble around the surface of carbon microfibers via physico-chemical interactions, facilitating the dispersion of microfibers in the cementitious matrix. Finally, these microspheres along with the silica fume particles could potentially act as microbridges between carbon microfibers and mortar matrix, and consequently improve the ability of the composite to absorb the fracture energy when under mechanical loading.

Conclusions

SPSM of 0.7 ± 0.5 μm in average diameter were successfully prepared and incorporated into the carbon microfiber-reinforced mortar specimens that were prepared

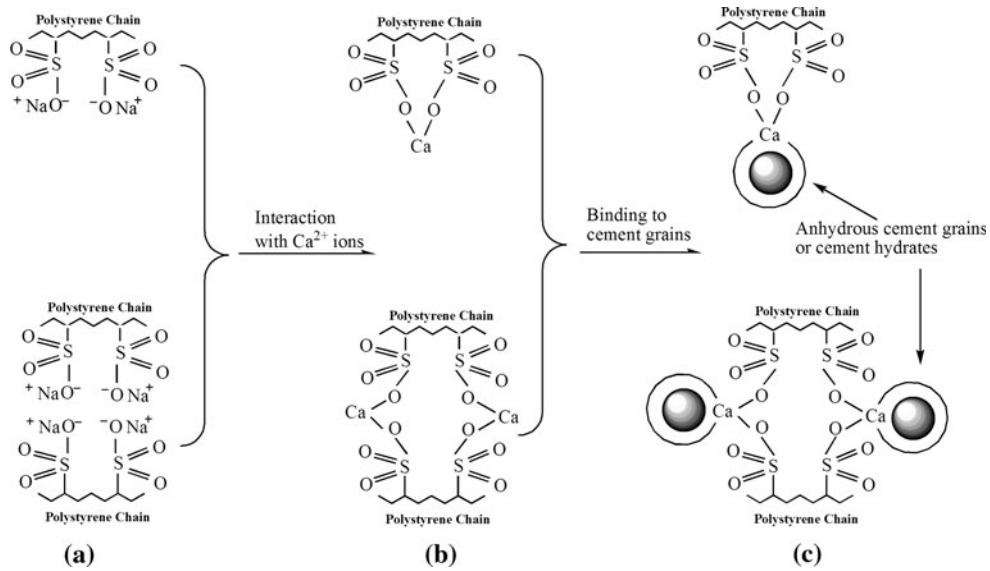

Fig. 9 Possible interactions between surface-sulfonated polystyrene microspheres with cement grains or cement hydrates

with silica fume at 15% by weight of cement, carbon microfibers at 2% by volume, water-to-binder ratio of 0.52, and sand-to-binder ratio of 2.

Various experiments were conducted to investigate the crack resistance of these cementitious composites with or without the SPSM admixed at 0.15% by weight of cement. The compressive strength and EIS data demonstrated that the incorporation of SPSM led to a denser and more refined microstructure of the cement mortar composite, likely attributable to the active interactions between SPSM and cement hydration products as well as carbon microfibers. The crack resistance of these cement-based composites was evaluated using a non-destructive test method under uniaxial compression loading along with a fatigue test under uniaxial compression cyclic loading. The data, in the form of critical stress, specific crack area, and fatigue strain, revealed that even at a small dosage the incorporation of SPSM into carbon microfiber-reinforced mortar retarded the initiation of unrecoverable microcracks and slowed down the propagation of microcracks under uniaxial compression loading, and improved the crack resistance and toughness of the specimens under fatigue loading.

While this exploratory research demonstrated the feasibility of using SPSM to enhance the crack resistance (and also load carrying capacity) of the carbon microfiber-reinforced mortar, more research is needed to optimize the combined use of SPSM and microfibers in "crack-free" concrete, in areas related to design, fabrication, characterization, and performance assessment.

Acknowledgements This work was supported by the Research and Innovative Technology Administration under the U.S. Department of Transportation through the University Transportation Center research grant. The authors would like to extend their appreciation to Dr. Xiaodong He for his previous effort put forth in this project and helpful discussions and Dr. Recep Avci of the Imaging and Chemical Analysis Laboratory at Montana State University for the use of FESEM instrumentation. We also greatly appreciate the gift of carbon microfibers from Kureha America Inc that was used in this work.

References

1. Li VC, Lepech M (2004) Crack resistant concrete material for transportation construction. Transportation research board 83rd annual meeting, transportation research board, Washington DC, compendium of papers (CD ROM), Paper No. 04-4680
2. Bentz DP, Weiss WJ (2008) Concrete Plant Int 3:56
3. Lange DA, Ouyang C, Shah SP (1996) Adv Cement Based Mater 3(1):20
4. Yi CK, Ostertag CP (2001) J Mater Sci 36(6):1513. doi:10.1023/A:1017557015523
5. Lawler JS, Zampini D, Shah SP (2002) ACI Mater J 99(4):379
6. Chung DDL (2000) Composites B 31(6–7):511
7. Ambrožič M, Vidovič K (2007) J Mater Sci 42(23):9645. doi:10.1007/s10853-007-1967-1
8. Sudin R, Swamy N (2006) J Mater Sci 41(21):6917. doi:10.1007/s10853-006-0224-3
9. Dalmay P, Smith A, Chotard T, Sahay-Turner P, Gloaguen V, Krausz P (2010) J Mater Sci 45(3):793. doi:10.1007/s10853-009-4002-x
10. McCarter WJ, Starrs G, Chrisp TM, Banfill PFG (2007) J Mater Sci 42(6):2200. doi:10.1007/s10853-007-1517-x
11. Xie P, Gu P, Beaudoin JJ (1996) J Mater Sci 31(15):4093. doi:10.1007/BF00352673
12. Ostertag CP, Yi CK (2007) Mater Struct 40(7):679
13. Van Gemert D, Czarnecki L, Maultzsch M, Schorn H, Beeldens A, Łukowski P, Knapen E (2004) Cement Concrete Compos 27(9):926
14. Kardon JB (1997) J Mater Civil Eng 9(2):85
15. Yang Z, Shi X, Creighton AT, Peterson MM (2009) Constr Build Mater 23(6):2283
16. Chen B, Liu J (2004) Cement Concrete Res 34(7):1259
17. Sussman V (1975) ACI J 72(7):321
18. Perry SH, Bischaff PH, Yamura K (1991) Mag Concrete Res 43(154):71
19. Ugelstad J, Söderberg L, Berge A, Bergström J (1983) Nature 303(5):95
20. Pappo J, Ermak TH, Steger HJ (1991) Immunology 73(3):277
21. Xu Z, Zhang Z, Zhang M (1999) J Dispers Sci Technol 20(6):1647
22. Loo YH (1992) Mater Struct 25(10):573
23. Shah SP, Chandra S (1968) ACI J 65(9):770
24. Hsu TTC, Slate FO, Sturman GM, Winter G (1963) ACI J 60(2):209
25. Lee MK, Barr BIG (2004) Cement Concrete Res 26(4):299
26. Hsu TTC (1984) Mater Struct 17(97):51
27. Yin W, Hsu TCC (1995) ACI Mater J 92(1):71
28. Song G (2000) Cement Concrete Res 30(11):1723
29. Torrents JM, Mason TO, Peled A, Shah SP, Garboczi EJ (2001) J Mater Sci 36(16):4003. doi:10.1023/A:1017986608910
30. Cabeza M, Merino P, Miranda A, Nóvoa XR, Sanchez I (2002) Cement Concrete Res 32(6):881
31. Shi X, Yang Z, Nguyen TA, Suo Z, Avci R, Song S (2009) Sci China Ser E 52(1):52